Behaviour of RC frame with strong masonry infill in response to cyclic horizontal loading

Sigmund, Vladimir; Zovkić, Jurko; Guljaš, Ivica

ISSN 1330-3651 (Print), ISSN 1848-6339 (Online)
UDC/UDK 624.012.45.072.33.04.046:519.87

BEHAVIOUR OF RC FRAME WITH STRONG MASONRY INFILL IN RESPONSE TO CYCLIC HORIZONTAL LOADING

Vladimir Sigmund, Jurko Zovkić, Ivica Guljaš

Original scientific paper
This paper gives an overview of the experimental results obtained by testing three reinforced concrete (RC) frame models with strong infill walls and one bare RC frame model for comparison. The experimental results of the RC frame models with and without a strong masonry infill are presented in terms of the collapse mechanism, lateral resistance, lateral stiffness and hysteretic energy. Based on those results, we obtained the ductility coefficients, behaviour factors, and equivalent damping coefficients of the RC frames with strong infill walls ("frame-wall") and the bare RC frame, all of these variables depending on storey drifts. The experimental and analytical results of frame-wall and RC frames, regarding their lateral capacity and lateral stiffness, were compared. Experiments showed that the masonry infill contributed to the lateral capacity, lateral stiffness, hysteretic energy, changed behaviour, as well as the equivalent damping coefficient of RC frames. It is shown that "frame-wall" composite behaved as full-fledged building type having lower vulnerability than RC frames and enough displacement capacity to sustain displacement cycles in the nonlinear range of response.

Keywords: *reinforced-concrete frame, strong infill wall, cyclic loading, experimental results, analytical results, comparison*

Ponašanje a-b okvira s jakim zidnim ispunom na horizontalno cikličko opterećenje

Izvorni znanstveni rad
U radu je dan prikaz eksperimentalnih rezultata tri ispitivana modela armirano-betonskih okvira (a-b) s jakim zidnim ispunama ("uokvireno zide") i jednog modela praznog a-b okvira. Prikazani su eksperimentalni rezultati u pogledu mehanizma sloma ispuna, poprečne nosivosti, poprečne krutosti kao i histereznih energija. Na osnovu eksperimentalnih rezultata dobiveni su koeficijenti duktilnosti, faktori ponašanja i koeficijenti ekvivalentnog prigušenja uokvirenog zida i praznog a-b okvira u ovisnosti o nivou relativnog katnog pomaka. Utvrđene su razine oštećenja zidnog ispuna koje su povezane s nivoima relativnih katnih pomaka. Eksperimentalni rezultati, dobiveni na uokvirenom zidu, uspoređeni su s analitičkim rezultatatima iz literature, glede poprečne nosivosti i poprečne krutosti. Iz eksperimentalnih rezultata vidljiv je doprinos zidnog ispuna na poprečnu nosivost, poprečnu krutost, histerezne energije, koeficijent duktilnosti, faktor ponašanja, i na koeficijent ekvivalentnog prigušenja u odnosu na prazan a-b okvir. Uokvireno zide može se korisiti kao ravnopravan nosivi element za preuzimanje horizontalnih opterećenja, unutar ograničenja promatranih parametara.

Ključne riječi: *analitički model, armirano-betonski okvir, cikličko opterećenje, eksperimentalni rezultati, jaki zidni ispun, usporedba rezultata*

1 Introduction

Reinforced concrete (RC) frame structures filled in with brick masonry walls are commonly used in low and medium-high buildings in the Republic of Croatia. Infill walls primarily serve architectural purposes and demands, while their constructive contribution is ignored; thus, the wall should be detached from the frame. This kind of construction is very rare, and usually the infill is glued to the frame or is even used as its form work. However, the composite behaviour of the infill and frame often remains unconsidered, as a consensus by the research community on the effects of masonry infill has not yet been reached [1]. Indeed, testing these structures is quite active, as shown by a number of recent experiments [2, 3, 4]. Besides having some adverse effects, these structures often exhibit increased stiffness, strength, and dissipation capacity along with decreased displacement and second-order effects. Nevertheless, design provisions for new frame-masonry buildings, as in EN 1998-1 [5], are mainly devoted to avoiding any potential consequences of infill wall; however, it does not account for the benefits of their contribution. EN 1998-3 [6] does not include any provisions that consider infill, even as a strengthening intervention, when evaluating the safety of existing buildings. Thus, this article as well as the works cited deal with RC frame structures designed for some lateral action while disregarding the influence of masonry infill. Frame-wall structures are composite structures made of an RC frame and masonry infill. These structures are often divided into weak and strong categories without clear distinction. A strong frame typically means a frame designed for seismic actions that has the following characteristics: strong columns – weak beams; small spacing of transverse reinforcement in columns, beams, and their connections; higher compressive strength of concrete. The strength of the masonry infill almost always refers to its compressive strength, which can be roughly divided into soft, medium, and strong categories. The failure mechanism and ductility of frame-masonry buildings depend on additional factors such as geometry (bay span to height ratio), relative stiffness and strength of the frame and masonry infill, ductile detailing of the frame, reinforcement of the infill when the infill controls the failure and on the infill distribution in the building plan and the elevation of the building. If brittle inelastic effects can be prevented (e.g. extensive cracking of the infill, bond-slip failure in the frame, or shear failure in frame members), then stiffness degradation and strength deterioration under cyclic loading are acceptable [7, 8]. The designs of contemporary earthquake-resistant structures should reliably limit damage in low and medium-strong earthquakes and prevent collapse during strong earthquakes. The goal of these designs is to meet customer requirements with rationally designed and constructed buildings for a given level of reliability. Thus, this research will contribute to a better understanding of the composite behaviour of RC frames and masonry infill.

2 The physical model

2.1 Introduction

To obtain the RC frame test model, we chose a common seven-storey reinforced-concrete office building (prototype) [9, 10]. The prototype was selected in order to obtain its cross-sectional dimensions (columns and beams), span, and height, as well as to determine the required/selected reinforcement in the columns and beams, as well as the corresponding vertical load, which simulates the load from the upper floors. The actual dimensions of the prototype are scaled in order to produce the corresponding test model.

In this paper, a model represents either a bare RC frame or an infilled RC frame test structure. This study is a part of the Croatian project "Seismic design of infilled frames", in which a total of ten models were created and tested [9]. The results of four models: three RC frame models with strong masonry infill built with commonly used hollow clay block masonry units and one bare RC frame model for comparison are presented in this paper. All models used in this report are designed and constructed at a 1:2,5 scale (Fig. 1).

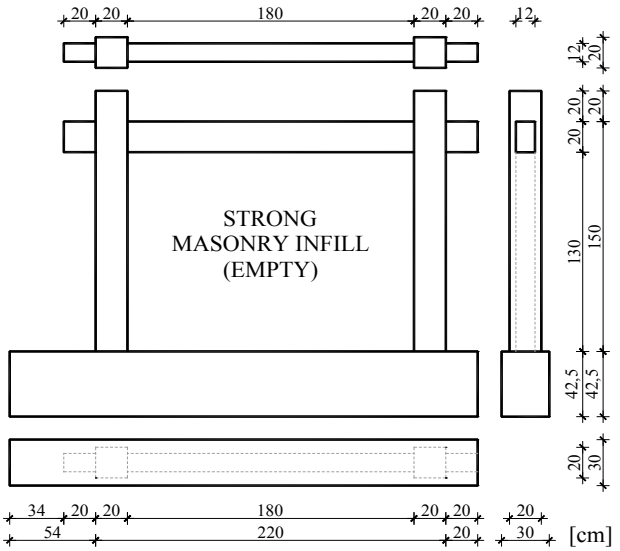

Figure 1 Scaled model of the reinforced-concrete frame

2.2 Models data

2.2.1 Reinforced-concrete frame

The models of the reinforced-concrete frames were made at a 1:2,5 scale based on a prototype, which represents the middle ground floor bay from the middle frame of the prototype [9, 10, 11, 12]. The specimens were produced as practical true models meaning that the prototype and the models had the same material properties and the same axial stress in the columns, thus simulating the loading from the upper floors. All the RC frame models were designed and constructed to comply with the C30/37 concrete strength class and the B500B reinforcement grade according to the Eurocodes [5, 6, 13]. Geometric and reinforcement details of the specimens are shown in Figs. 1 and 2.

The longitudinal reinforcement ratio of the columns was ρ_v = 2,36 %, while for the beams was ρ_v =1,31 % in the mid-span and ρ_v =3,27 % at their ends.

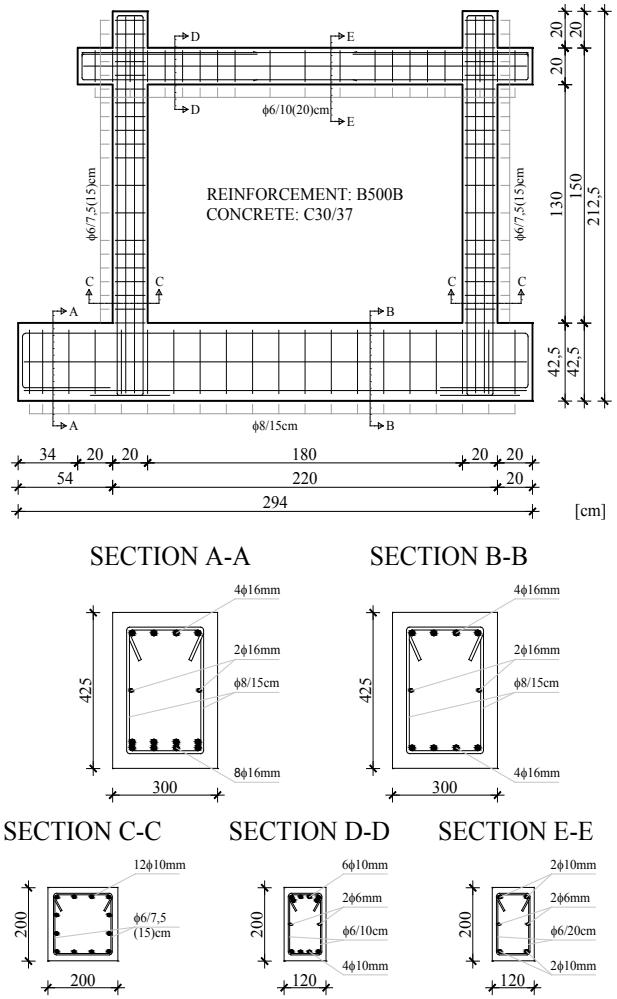

Figure 2 Geometric and reinforcement details of the model specimens

A concrete cube samples were taken from each frame and the mechanical properties of the concrete (mean compressive strength, f_{ck}) were obtained according to the norms [13]. The concrete tensile strength, $f_{ct,m}$, and the modulus of elasticity, E_{cm}, were obtained by using the equations [13]:

$$f_{ct,m} = 0{,}3 \cdot f_{ck}^{\,2/3}, \tag{1}$$

$$E_{cm} = 9500 \cdot (f_{ck} + 8)^{1/3} \ . \tag{2}$$

The mechanical properties obtained from the concrete samples are shown in Tab. 1.

Table 1 Mechanical properties of concrete

RC frame model	Compressive strength, f_{ck} / N/mm^2	Tensile strength, $f_{ct,m}$ / N/mm^2	Modulus of elasticity, E_{cm} / N/mm^2
K-7	41,50	3,60	34 881
K-5	51,50	4,15	37 088
K-8	43,50	3,71	35 345
K-9	35,00	3,21	33 282

The mechanical properties of the reinforcement used in the models were obtained by tensile tests on three reinforcement bars with diameters of 8, 10 and 12 mm, all

in accordance with the corresponding norms. All tests were carried out in the Laboratory for Experimental Mechanics at the Faculty of Civil Engineering in Osijek. The results are presented in Tab. 2.

Table 2 Mechanical properties of reinforcement

Rebar diameter, Φ / mm	Yield strength, mean value f_y / N/mm^2	Tensile strength, mean value f_u / N/mm^2	Modulus of elasticity, mean value E/ N/mm^2
8	583	654	201 385
10	594	700	206 957
12	574	605	198 599
Mean values	**584**	**653**	**202 314**

2.2.2 Masonry infill

The masonry infills were produced by hollow clay masonry units V-5 that belonged to Group 2 under Eurocode 6 with a nominal compressive strength of 15 MPa. The mechanical properties of masonry units, mortar and masonry wallets were tested according to the European norms, and are presented in Tab. 3.

Table 3 Mechanical properties of the mortar

Type of test	Mean tensile strength, $f_{mt,sr}$ / N/mm^2	Mean compressive strength, $f_{mc,sr}$ / N/mm^2
Masonry units	7,80	38,39
Wallets/compression tests	1,09	5,13
Wallets/ shear tests	1,33	6,02
Infill wall tests	1,26	5,11

The compressive strength of masonry units was tested on six randomly selected elements with prepared units' pressed surfaces. The units were prepared for testing by using cement mortar with mechanical properties listed in Tab. 3.These results showed that the masonry units had a mean compressive strength of $f_{mc,sr}$=$f_{b,sr}$=13,21 N/mm^2.

The compressive strength of the masonry infill samples (wallets) were tested in accordance with EN1052-1:1998[14, 15]. Masonry panels were built with hollow clay masonry units connected with lime-cement mortar produced in-situ in volume proportions of 1:1:5 (lime:cement:sand). The bed joints were 10 mm thick and the head joints were completely filled. Three masonry wall samples (wallets) were tested.

The initial shear strength of the masonry infill was determined in accordance with prEN1052-3:2001 [14, 15], and the measured mechanical properties are listed in Tab. 4.

Table 4 Mechanical properties of masonry infill walls

Mean compressive strength, $f_{cw,sr}$ / N/mm^2	2,62
Mean modulus of elasticity, E / N/mm^2	6572
Mean initial shear strength, f_{vo} / N/mm^2	0,536
Mean internal friction coefficient, α / °	22,17

The masonry infill wall panels were produced with scaled masonry units cut from the original panels, preserving the amount and area of the holes (with the same percentage of voids) and the same number of bed joints. The dimensions of the scaled wall elements are shown in Tab. 5.

Table 5 Dimension of scaled wall elements

Type of infill wall element	Dimensions of original infill wall elements, $l_u/w_u/h_u$ / mm	Dimensions of scaled infill wall elements, $l_u/w_u/h_u$ / mm
Brick block MO10	250/190/190	190/120/90

The masonry infill wall panels were produced with general purpose lime-cement mortar made "in situ" with a volume proportion of cement:lime:sand=1:1:5 and with the bed and head-joint thicknesses of 10 mm.

Figure 3 Construction of infill walls

2.2.3 Test models

All tested specimens were divided in two groups, as shown in Tab. 6, in order to simplify their identification and interpretation and analysis of the results.

Table 6 Test models

Group	Model	RC frame model	Infill type
GROUP I	MODEL7	K-7	Brick block MO10 (strong infill)
	MODEL8	K-5	
	MODEL9	K-8	
GROUP IV	MODEL10	K-9	No infill

3 Testing of the specimens

3.1 Introduction

Model testing was performed in a closed steel frame, as shown in Fig. 4. The steel testing frame was horizontally supported with braces in order to prevent horizontal movement. The test setup (steel frame and corresponding braces) was connected to the strong floor.

Cyclic lateral load was applied to the beam ends of the specimen by using two double-acting hydraulic jacks fixed to the steel columns of the test frame. The specimens were adequately insured against adverse developments (i.e. out of plane behaviour). Vertical load was applied to the tops of the columns by using two hydraulic jacks placed on a carriage wheel, which allowed them to move horizontally and prevented their rotation (Fig. 4).

The foundation beam of each specimen was fixed to the steel frame and to the strong floor.

3.2 Measuring devices

Measuring devices were placed on all models (groups) in the same manner as that shown in Fig. 4.

Displacements were measured with Linear displacement velocity transducers (LVDT), forces with force transducers: horizontal (FORCE_HL and FORCE_HD) and vertical (FORCE_VL and FORCE_VD), as is shown in Fig. 4.

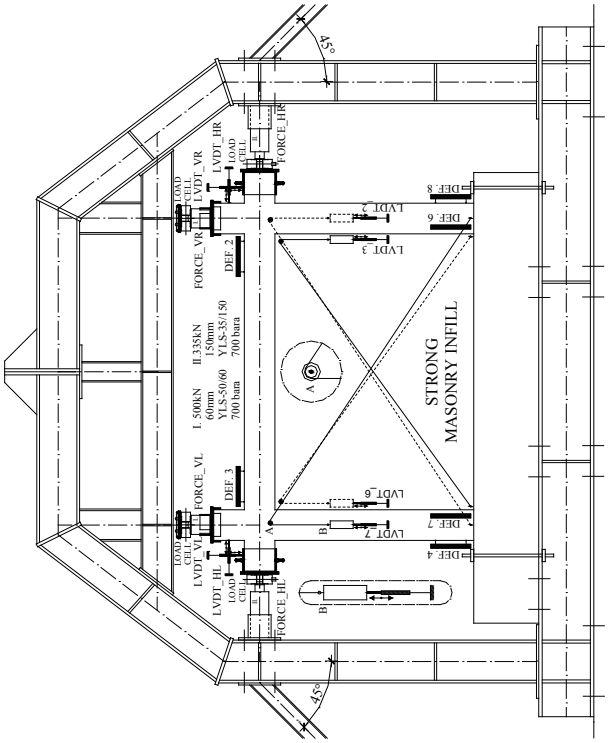

Figure 4 Test setup

The vertical and horizontal displacements of the specimens were measured at the beam and columns ends by displacement transducers (vertical LVDT_VL and LVDT_VD and horizontal LVDT_HL and LVDT_HD) attached to separate scaffolding, detached from the closed steel frame, in order to measure the absolute displacements. Deformations of the diagonals were measured on the frame and on the infill panels by strain gauges.

All data from the measuring instruments were collected with two Dewetron measurement systems and were analysed using DEWEsoftver.6.6.7 software.

3.3 Test loadings

The vertical load simulated loading from the upper floors was applied to the tops of the columns by two hydraulic jacks, with 500 kN capacity each. Designed magnitudes of the vertical loads in prototype were scaled to $1{:}2{,}5^2$ for the specimens' loading. In that way the axial stress in the columns was the same in the Prototype and Model. In Tab. 7, designed and achieved axial loads in the columns are presented.

Table 7 Vertical loads

Group	Designed axial load N_{mi} / kN	Achieved mean axial load, $N_{mi,d}$ / kN
GROUP I	362	357
GROUP IV	354	346

A cyclic horizontal (lateral) load was applied by using two double-acting hydraulic jacks, with a 350 kN capacity, each. This load was increased in 10 kN steps until the specimen yielded. At this point, the load was increased so that the lateral displacement increased in 1mm steps (Fig. 5). Once the masonry infill was severely damaged, we applied a lateral load from only one side until the masonry infill was heavily damaged.

The vertical loads were not entirely constant during the tests (Fig. 5). Differences to the designed values occurred due to the boundary conditions and they were corrected by pressure valves. Any differences in the horizontal forces were within the permissible range.

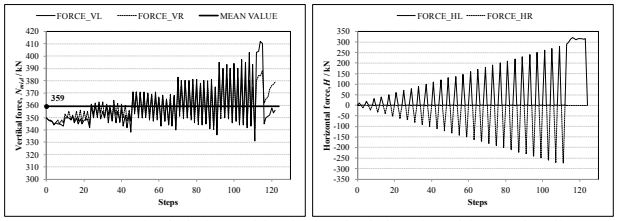

Figure 5 Vertical (left) and horizontal (right) time history loadings (MODEL 7)

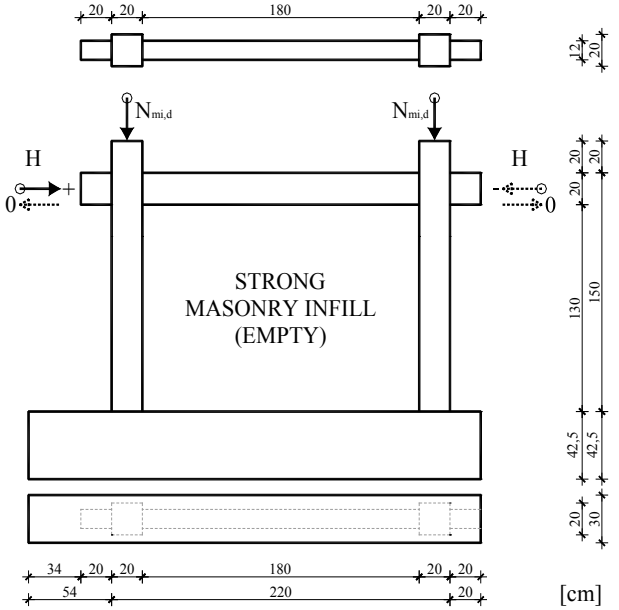

Figure 6 Vertical (N) and horizontal (H) model loads

4 Test results

The obtained results from the specimens' tests are presented for the model dimensions and loads. Presented are the crack patterns, corresponding failure mechanism, the cyclic experimental response curves (hysteresis loops) and the obtained primary curves (resistance envelope curves) for the cyclic lateral loading.

4.1 Crack patterns and the infill's failure mechanism

The final crack patterns of the specimens at drift levels of 0,98 to 1,34 % are shown in Figs. 7 ÷ 9. For the specimens in GROUP I, the cracks spread (advance) diagonally along the vertical and horizontal joints; thus, the shear strength of these models depended on their mortar joints. Notably, the horizontal cracks in these

models prevented the formation of diagonal cracks in the upper half of the infill wall.

At higher loads a notable separation between the infill wall and the frame elements appeared. Eventually, the masonry infill crushed at the beam-column joints and parts of masonry units fell out. The failure mechanism could be described as a combination of shear-sliding and diagonal-tension failure. Finally, tensile cracks appeared at the columns' toes. By correlating the forces and corresponding displacements at particular damage levels, we found out that first cracks in GROUP I always occurred at storey drift values near 0,05 %. Their maximum capacity was achieved at storey drifts of 0,25 ÷ 0,30 %.

The interstorey drift, *IDR*, was calculated for both GROUPS as the mean value of horizontal LVDT readings (strain gauges) according to the expression:

$$IDR=\{[(LVDT\_HL+LVDT\_HD)/2]\times 100\}/1500\ (\%), \quad (3)$$

where:
LVDT_HL, LVDT_HD, according to Fig. 4, 1500 is model height (mm).

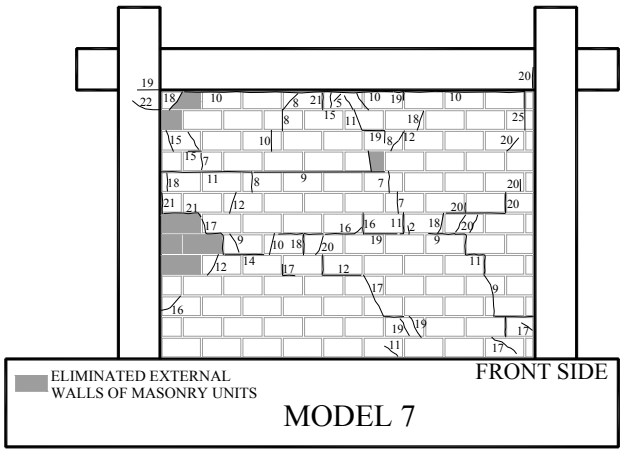

Figure 7 Final crack pattern for MODEL 7 (*IDR*=1,10 %)

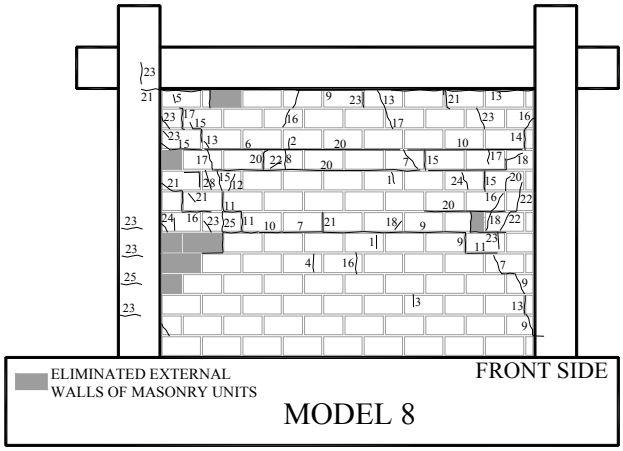

Figure 8 Final crack pattern for MODEL 8 (*IDR*=0,98 %)

For the specimen in GROUP IV (RC bare frame), cracks appeared at the columns' toes, on both columns. When the lateral force was increased, cracks widened, and plastic hinges in the vicinity of the foundation beam-column joints were formed. At higher horizontal forces, cracks appeared in the beam-column joints of the frame. Photographs of the cracks in the bare RC frame are shown in Fig. 10.

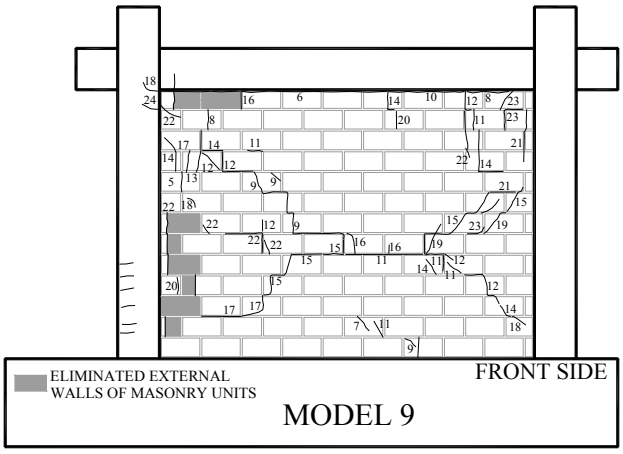

Figure 9 Final crack pattern for MODEL 9 (*IDR*=1,34 %)

Figure 10 Crack patterns observed on the MODEL 10 columns

4.2 Hysteretic behaviour

The measured hysteretic relationships between the lateral load and displacement of the specimens are presented in Figs. 11 ÷ 14, together with the primary curves (resistance envelope curves) for horizontal force and displacement. On the secondary axes presented are the base-shear ratios (measured base shear in relation to the total weight of the model) as well as the storey drifts.

The hysteresis loops for each model were calculated as the mean horizontal displacements according to the expression (4)

$$d=(LVDT\_HL+LVDT\_HD)/2\ (\text{mm}), \quad (4)$$

while the inter storey drift ratio, *IDR*, was calculated for each model according to expression (3).

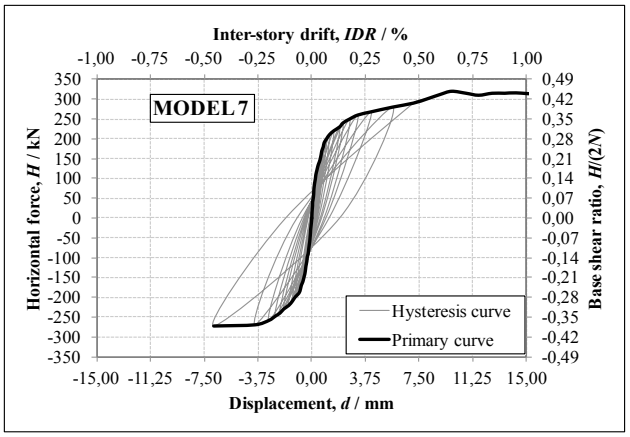

Figure 11 Lateral load – displacement curve of the Model 7

Each primary curve was obtained as the envelope of the peak values of the corresponding hysteresis loops.

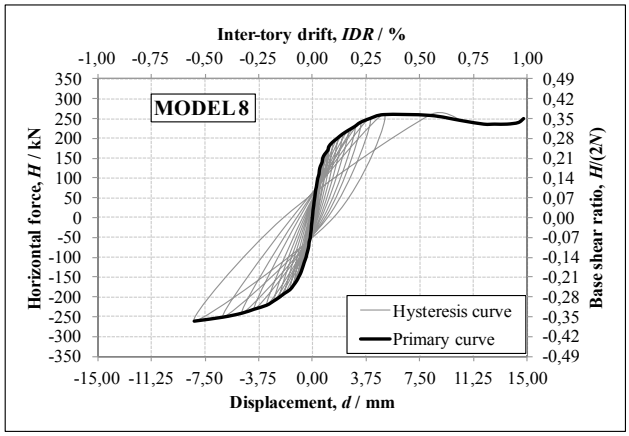

Figure 12 Lateral load – displacement curve of the MODEL 8

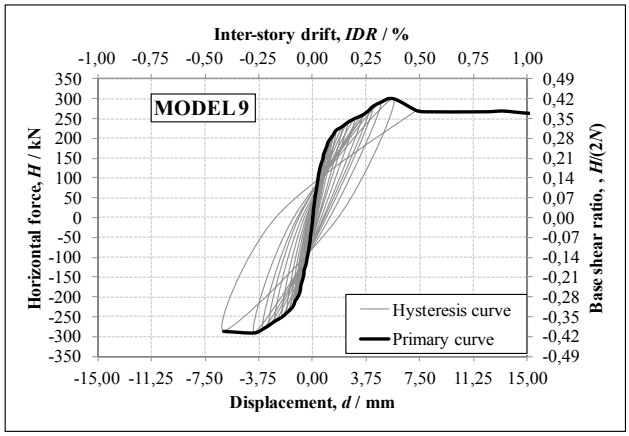

Figure 13 Lateral load – displacement curve of the MODEL 9

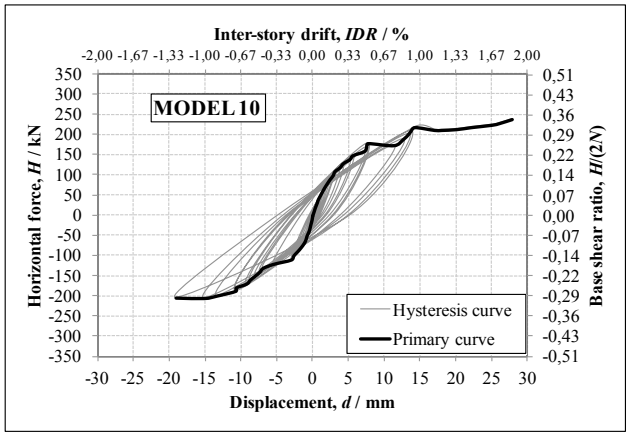

Figure 14 Lateral load – displacement curve of the MODEL 10

In Figs. 15 and 16 shown are the primary curves of each tested model as well as their averaged optimized primary curve that describe the behaviour of the group. The optimized curve represents only the positive branches of the primary curves for model sets. It was obtained by the MATLAB ver. 2013 "Optimal Fit of a Non-linear Function" method. This method finds the optimal fit of non-linear functions from a data set by using the FMINSEARCH function, which implements the Nelder–Mead simplex algorithm (direct search) to reduce the nonlinear function with several variables. Its goal is to find a function y with two linear and two nonlinear parameters for the measured data according to (5).

$$y = C(1) \cdot \exp(-\lambda(1) \cdot t) + C(2) \cdot \exp(-\lambda(2) \cdot t) \,. \tag{5}$$

For the vertical load, the mean of the actual vertical loads on each model group was taken, as shown in Tab. 7.

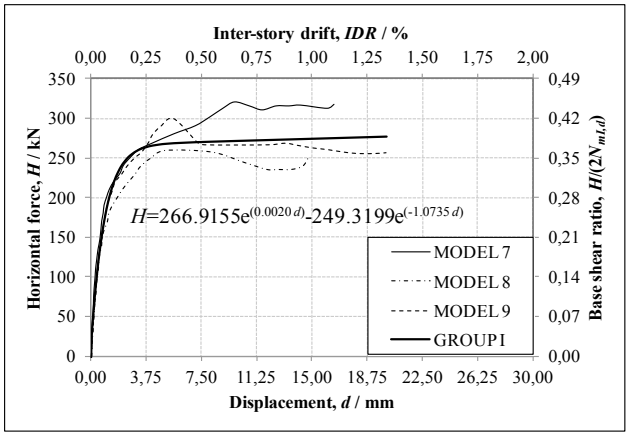

Figure 15 Primary curves for models in GROUP I and the optimized primary curve

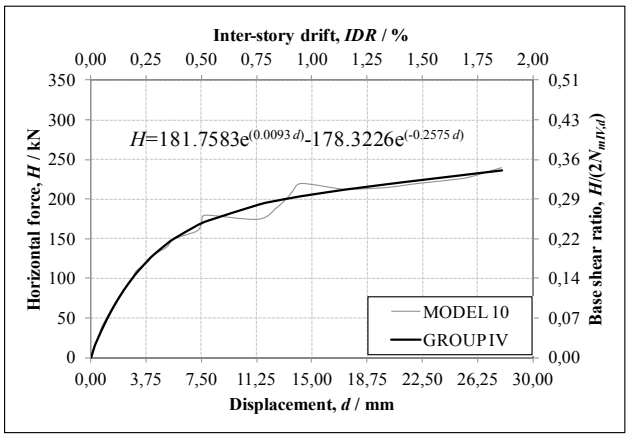

Figure 16 Primary curves for model in GROUP IV and the optimized primary curve

4.3 Lateral strengths

From the compared optimized curves shown in Fig. 17 it is obvious that the lateral stiffness of the frames with infill was much higher than that of the bare frame, especially at lower drift levels.

The initial linear portion of the primary curve reveals that the infilled frames acted as composite "framed-masonry" element, up to drifts of about 0,1 %. As the infill and the frame separated from each other, the infill and the frame elements were damaged, and system stiffness decreased gradually until the resistance reached its maximum value (H_{max}) at drifts of 0,25 ÷ 0,30 %. After that point an almost horizontal force-deformation relationship followed (yielding) up to the moment when the frame overtook the lateral carrying capacity.

The details of that branch depended on the degradation process of the infill, indicating that the RC frame took on an increasing portion of the overall capacity. In all tested specimens, the first cracks appeared at drifts of about 0,05 % and their behaviour was

essentially linear-elastic. The systems retained their load-carrying capacity up to drifts of 0,5 % with much lower stiffness. The results presented in Fig. 15 show that frames with infill retained their load-carrying capacities up to drift ratio of about 1 %, at which point the infill contribution was completely lost and the infill was heavily damaged. Above that drift level, the positive contribution of the infill was lost, and a negative contribution could dominate if the RC frame elements were not properly designed for shear. MODEL 10 (bare-frame specimen) was much more flexible at small drifts, but retained its lateral load-carrying capacity up to drifts of about 2 % (Fig. 16).

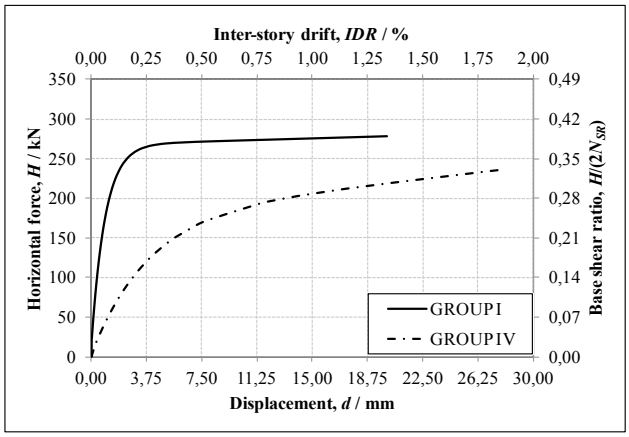

Figure 17 Comparison of the primary curves of GROUP I and GROUP IV

The base shear capacity of the "framed-masonry" structure related to that of the bare frame is presented in Tab. 8 for various drifts.

Table 8 Lateral load capacity, H / kN, at certain drifts (displacements)

IDR / %	0,10	0,25	0,50	0,75
GROUP I	219 (3,43)	264 (2,17)	271 (1,60)	273 (1,42)
GROUP IV	64 (1,00)	122 (1,00)	169 (1,00)	193 (1,00)
IDR / %	0,83	1,34	1,68	1,86
GROUP I	273 (1,39	278 (1,27)	–	–
GROUP IV	197 (1,00)	218 (1,00)	230 (1,00)	236 (1,00)

If we normalize the capacity of the bare frame as 1, the capacity of the MODEL 8 for a 0,1 % drift was 2,8 times bigger, and so on. The infill contribution, which decreased with increased drift, was about 30 % for a 1 % drift, although the masonry wall was severely damaged and started to fall out of the plane.

4.4 Idealization of experimental results

The experimental resistance envelope curves (primary curves) are represented by a bi-linear idealisation in Figs. 18 and 19. To idealise the experimentally obtained primary curve, we used the equations for calculating the lateral resistance and deformability of confined masonry walls as described in Tomaževič [16].

Three limit states of the idealised experimental envelopes were determined as:

1 – Crack limit, corresponding to a displacement at the formation of the first significant cracks in the wall, as a fraction of the maximum resistance (H_1/H_{max}=0,60 and 0,05 % storey drift);

2 – Ultimate resistance calculated by equalizing the areas under the experimental load curve and the bilinear idealisation curve;

3 – Ultimate state, determined by maximum displacement attained during actual test.

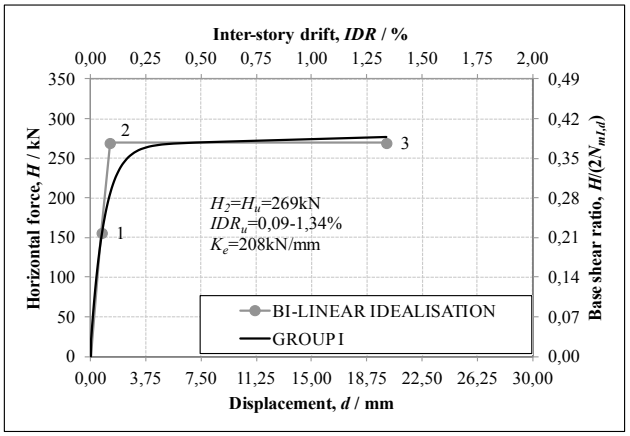

Figure 18 Idealisation of the primary curve for GROUP I

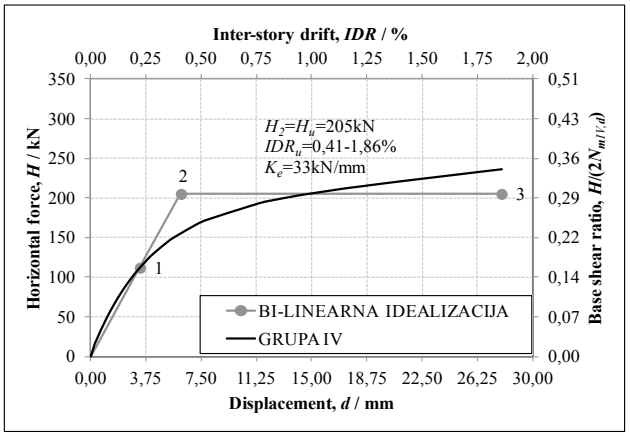

Figure 19 Idealisation of the primary curve for GROUP IV

Structural performance beyond the elastic range is usually expressed in terms of the ductility ratio, μ. Because the lateral resistance never decreased under 90 % of the H_{max}, we calculated the displacement ductility ratio as the ratio between the displacement at which the infill was heavily damaged and the idealised yield displacement, i.e. according to (6):

$$\mu = d_3 / d_2 . \tag{6}$$

The obtained ductility ratios of each group, based on bilinear idealisation of the experimental results, are presented in Tab. 9. We set the ultimate displacement to be the moment when the infill lost its integrity while the reinforced-concrete frame remained almost intact. The structural behaviour factor, q, shows that the infill walls contributed notably and that all tested specimens performed well under lateral loads simulating earthquake forces. These values are close to those suggested for RC

wall structures. The behaviour factor was calculated according to the expression (7):

$$q = \sqrt{2 \cdot \mu - 1} \ . \tag{7}$$

Table 9 Ductility ratios and the behaviour factors of specimens at various drift ratios

IDR	0,50 %		0,75 %		0,83 %	
Group	μ	q	μ	q	μ	q
GROUP I	5,79	3,25	8,68	4,05	9,61	4,28
GROUP IV	1,22	1,20	1,84	1,63	2,03	1,76
IDR	1,34 %		1,68 %		1,86 %	
Group	μ	q	μ	q	μ	q
GROUP I	15,11	5,47	–	–	–	–
GROUP IV	3,28	2,36	4,11	2,69	4,55	2,85

4.5 Lateral stiffness

The secant stiffness degradation values of our specimens are presented in Fig. 20. It was computed for each drift level and normalised with the initial pre-cracked stiffness (stiffness at the onset of the first cracks) using the optimized primary curves of each group. The initial stiffness, K_0, for GROUP I was calculated as the stiffness at a storey drift of 0,05 % and 0,22 % for GROUP IV (RC bare frame), respectively. The initial stiffness was an elastic stiffness (K_0=K_e) with the values shown in Figs. 18 and 19.

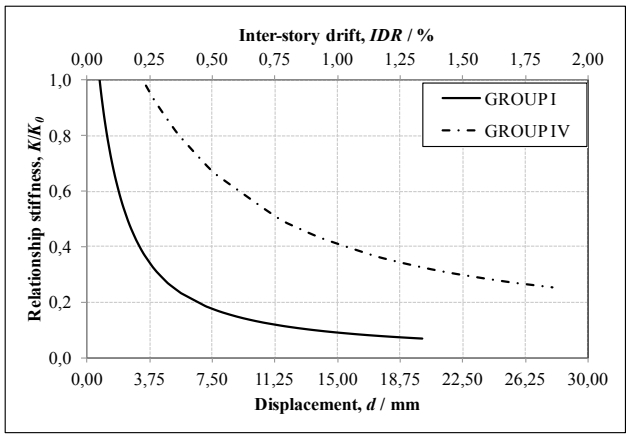

Figure 20 Degradation of stiffness for all specimens

Because the initial stiffness of the "framed-masonry" specimens (GROUP I) was much higher, they also exhibited more pronounced stiffness degradation compared to the bare-frame specimen (GROUP IV). This behaviour correlates well with the lateral strength of the specimens.

4.6 Hysteretic energy

The amount of the absorbed and dissipated hysteretic energy was calculated according to Fig. 21 [17]. Note that the dissipated energy was calculated as the cumulative area within the hysteresis curve for each cycle up to a particular storey drift.

The amount of absorbed energy in each group as a function of storey drift is shown in Fig. 22. "Framed-masonry" specimens absorbed more energy (GROUP I) than the bare RC frame (GROUP IV) specimen. The amount of the absorbed energy notably increased with increase of the storey drifts in all groups. Addition of the masonry infill within the RC frame improved the energy absorption capacity of the frame.

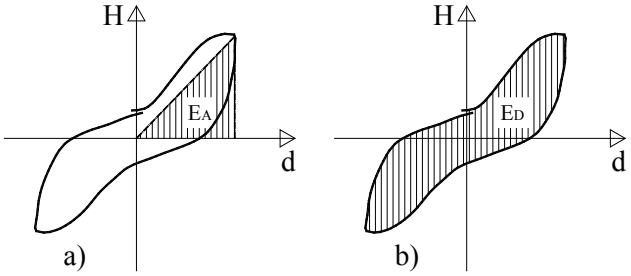

Figure 21 Determination of the a) absorbed energy and b) dissipated hysteretic energy

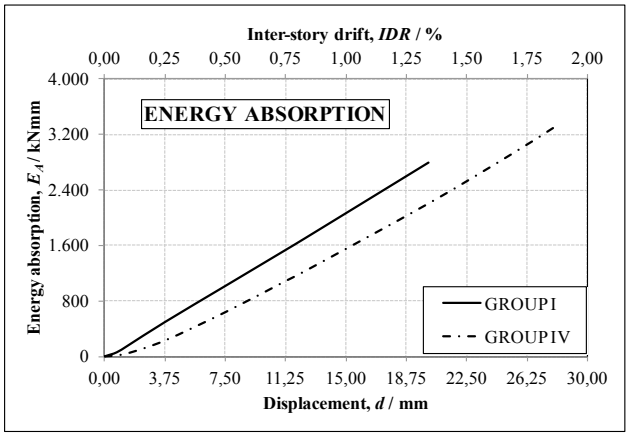

Figure 22 Energy absorption at various drifts for both groups

The same conclusion applies for the energy dissipation in Fig. 23.

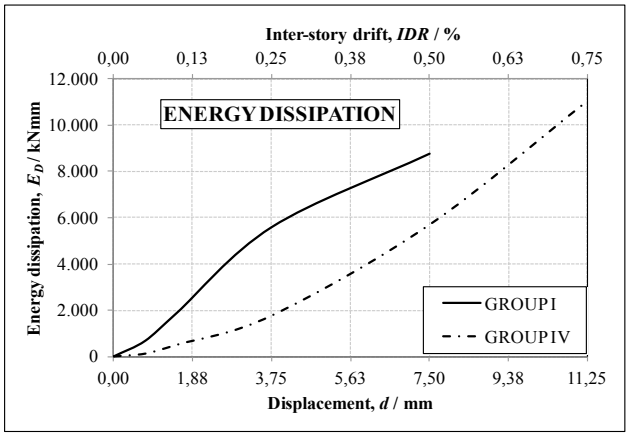

Figure 23 Energy dissipation at various drifts for both test groups

Based on earthquake-simulation testing of RC structures modelled as single-degree-of-freedom (SDOF) systems (SDOF), Gulkan and Sozen (1976) concluded that it was possible to describe the inelastic response of the RC structure as an elastic SDOF system with reduced stiffness and increased damping, calculated by using the following expression:

$$\xi_e = 0{,}2 \cdot \left(1 - 1/\sqrt{\mu}\right) + 0{,}02 \ , \tag{8}$$

where μ is the displacement ductility ratio, calculated by using expression (6).

The damping coefficients as functions of the ductility coefficients at various storey drifts are shown in Fig. 24. They increase with increase in ductility and storey drifts. Additionally, Fig. 24 shows that the contribution of the infill wall (GROUP I) to the damping coefficient was significant compared to the bare RC frame (GROUPIV).

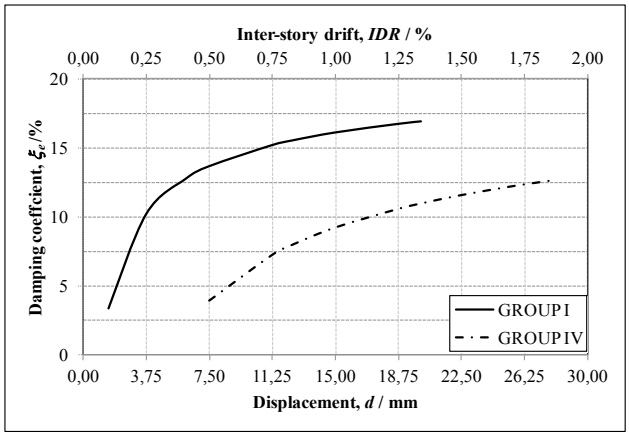

Figure 24 Damping coefficient as a function of drift levels

4.7 Damage grades of the masonry infill wall

Based on the experimental results analysed and according to the categorized damage levels, as suggested in EMS98 and some other available methods, we classified the damage according to the storey drifts.

On the basis of the observed damage levels (onset of cracks in the infill wall, separation between the infill and RC frame, fallout of wall fillings, etc.), we defined storey drift levels with corresponding damage classifications in Tab. 10.

Table 10 Damages and drift ratios according to EMS98

Drift ratio, *IDR* / %	Structural damage description	Technical and economical feasibility of repair	Damage level, *S* / °
0,0<*IDR*<=0,1	Insignificant	Repairable	1°
0,1<*IDR*<=0,3	Moderate	Repairable	2°
0,3<*IDR*<=0,5	Moderately difficult	Repairable	3°
0,5<*IDR*<1,0	Extensive	Repairable	4°
IDR>=1,0	Excessive, collapse	Irreparable	5°

5 The analytical model

5.1 Introduction

The RC frames with masonry infill have recently been intensively investigated [15, 16, 18]. The results presented in this paper (as well as from previous literature) showed that the composite "framed-masonry" structure had much higher stiffness, especially at smaller drifts, and higher base shear capacity (that depended on the infill strength and infill/frame relationship) than the bare frame structure and absorbed and dissipated more hysteretic energy. However, higher stiffness also leads to the increase of demand when the system becomes exposed to seismic loadings. The seismic capacity of "framed-masonry" structures depends on a number of factors, including size of the elements, quality of concrete and rebars, quality and type of masonry units and mortar, construction quality of the infill wall, and details of the RC frame and infill wall connections.

5.2 Seismic capacity of the RC infilled frames according to the Slovenian research

Based on the previous experiments, Žarnić suggested two possible modelling assumptions for the inelastic behaviour of infilled-frames. The first model, which will be shown here [18], characterizes a response of the structure in terms of a load-displacement relationship, while the second model allows full dynamic analysis of the infill walls modelled with a set of diagonal springs. A three-part linear force–displacement relationship diagram is shown in Fig. 25, where:

H_{Rcr} − shear resistance of the RC infilled frame at the onset of the first cracks,

H_{Re} − shear resistance of the RC infilled frame at the time of separation between the infill wall and the RC frame,

H_{Ru} − ultimate shear force/capacity of the RC infilled frame,

K_i − initial stiffness of the RC infilled frame,

K_e − stiffness of the RC infilled frame at the time of separation between the infill wall and the RC frame,

K_u − stiffness of the RC infilled frame when the capacity is reached.

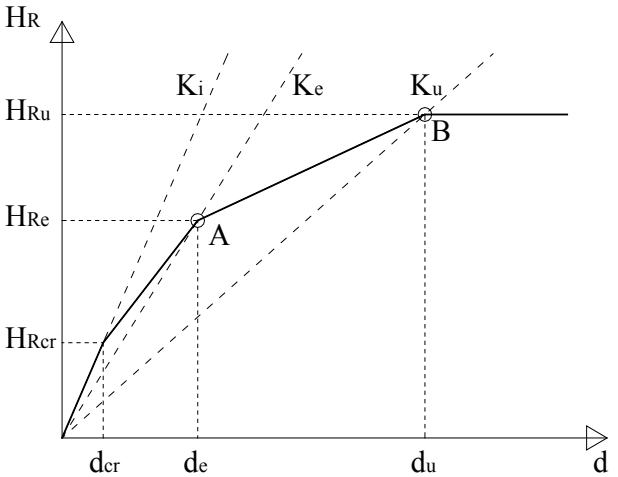

Figure 25 Linear idealisation of the structural behaviour of an RC infilled frame

Expressions for determining the above-mentioned parameters can be found in [10, 15, 16], as well as the necessary parameters for their calculation.

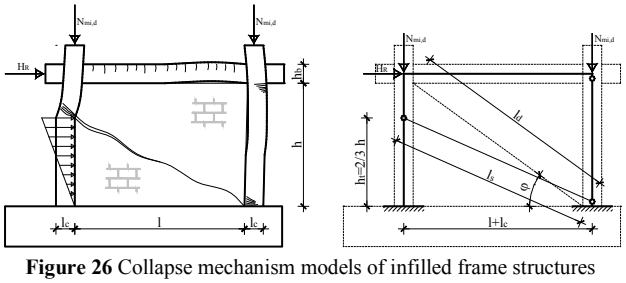

Figure 26 Collapse mechanism models of infilled frame structures

The stiffness of the RC infilled frame with large cracks, K_u, is calculated as the stiffness of the crack-free RC frame supported by a wall filled to 2/3 of its height (h_i= 2/3 h), as shown in Fig. 26.

The cross-sectional area, A_d, of the equivalent strut and its width, w, are calculated using expression (9). The geometric characteristics of the equivalent strut are shown in Fig. 27:

$$A_d = K_u \cdot (l_d / E),\ l_d = \sqrt{h^2 + l^2} \text{ and } w = A_d / t\ . \qquad (9)$$

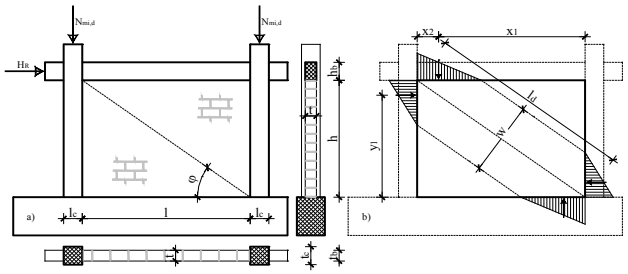

Figure 27 a) Test setup of the infilled frame model,
b) Idealised stress states in the vicinity of compression diagonal ends

5.3 Comparison of the analytical and experimental results

We compared the presented analytical results (especially ultimate lateral resistance and stiffness) with experimental results described by bi-linear idealized curves [15, 16], as shown in Fig. 28. Analytical results were good in predicting the ultimate lateral resistance with the error margin less than 5 %.

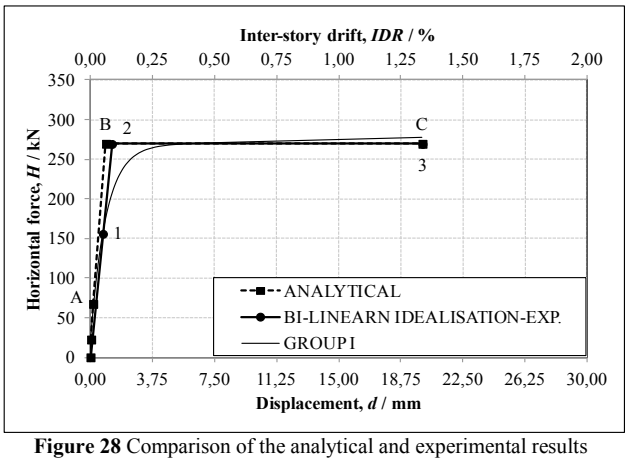

Figure 28 Comparison of the analytical and experimental results

In Fig. 28 and Tab. 11, the characteristic points are as follows:
$A = H_{Re}$ − yield force of infill wall under joint vertical and horizontal loads at low strain levels;
$B = H_{Ru}$ − ultimate lateral resistance of the infilled RC frame;
C − extended horizontal branch of point B up to the final experimentally determined storey displacement;
1 - lateral force at storey drift of 0,05 %, corresponding to the onset of the first significant cracks in the wall;
2 - ultimate lateral force obtained from bi-linear idealisation of the experimental curve;
3 - extended horizontal branch of point 2, up to the final experimentally determined storey displacement.

Table 11 Comparison of the lateral strength

Group	H_A/IDR kN / %	H_B/IDR kN / %	H_C/IDR kN / %
GROUP I	Analytical		
	67/0,01	270/0,06	270/1,34
	Experimental		
	156/0,05	269/0,09	269/1,34

The analytical model gave higher values for the lateral stiffness than those obtained experimentally. The differences are shown in Tab. 12.

Table 12 Comparison of the lateral stiffness

Group	Analytical	Experimental	Difference
	K_u / kN·mm	K_u=K_e / kN·mm	%
GROUP I	286,16	207,83	38

6 Conclusion

The masonry infill wall significantly contributed to the overall structural performance of the structure. We found that it significantly increased the stiffness, lateral strength, and absorbed and dissipated hysteretic energy of the RC infilled frame up to a storey drift of about 1 %.

Within conventional seismic design, which focuses on accelerations and strength, it may be difficult to recognize the benefits of increases in stiffness. However, research and field evidence has shown that increases in stiffness are beneficial because they lead to reductions in the magnitude of the deformations induced by ground motions.

Our experiments showed that the lateral resistance of the RC infilled frame ("framed-masonry") is much higher than that of the bare RC frame, especially at low storey drifts. The initial linear portions of the hysteresis envelopes (primary curves) indicate that the infilled frames act as composite "frame-masonry" elements. We observed the onset of the first cracks in all tested models at storey drift of about 0,05 %, a behaviour which was essentially linear-elastic. The systems retained their load-carrying capacity up to drift of 0,5 % with much lower stiffness. The frame-masonry composites retained their load-carrying capacities up to drift ratio of 1 %, at which point the infill contribution was almost completely lost and the infill was significantly damaged. After that drift level, the positive contribution of the infill could be neglected and the negative contribution could have dominated if the RC frame were not properly designed for shear.

As for the lateral stiffness, our conclusions correspond well with the one that correlates the lateral strength of the specimens. For cyclic loading, the secant stiffness of the infilled frame gradually approached that of the bare frame as the lateral load and corresponding drift level increased. In other words, the secant stiffness of the infilled frame decreased at displacement levels up to 1 % and above.

The amount of the absorbed and dissipated hysteretic energy in the "frame-masonry" system is much higher than in the bare RC frames, especially at small displacement levels.

The structural behaviour factor, q, and equivalent damping coefficient, calculated by using the ductility ratio, μ, shows the contribution of the infill walls and the good performance of all test models under lateral loads that simulate earthquake forces. Our obtained values can be used when designing a "frame-masonry" structural system to match an expected level of seismic behaviour.

Based on our experimental results, we classified the damage to the infill walls based on storey drift. By observing differing levels of damage to the infill walls across various storey displacement levels, we defined and classified a set of storey drift levels with corresponding damage levels. The experimental program has shown that frame-masonry composite has enough displacement capacity to sustain displacement cycles in the nonlinear range of response. If the idea of damage control is to be used for the frame-masonry composite, drift should be kept under 0,5 %.

Finally, we obtained analytical results based on existing research models of RC infilled frames. To simulate the local response of the masonry infill panel, we used the equivalent diagonal strut model. The initial analytical model gave very good results in terms of lateral capacity, while it failed to predict the expected horizontal displacements and drifts.

Acknowledgements

The research presented in this paper is a part of the research project "Seismic design of in-filled frames", no. 149-1492966-1536, supported by the Ministry of Science, Education and Sports of the Republic of Croatia, whose support is gratefully acknowledged.

7 References

[1] Mainstone, R. On the Stiffness and Strength of Infilled Frames. // Proceedings of the Institution of Civil Engineers, Supplement, 48, (1971), pp. 57-90.
[2] Colangelo, F. Pseudo-dynamic seismic response of reinforced concrete frames infilled with non-structural brick masonry. // Earthquake Engng. & Struct. Dyn. 34, (2005), pp. 1219-1241.
[3] Han-Seon, Lee; Sung-Woo, Woo. Effect of masonry infills on seismic performance of a 3-storey R/C frame with non-seismic detailing. // Earthquake Engng. & Struct. Dyn. 31, (2002), pp. 353-378 (DOI: 10.1002/eqe.112).
[4] Kakaletsis, D. J.; Karayannis, C. G. Influence of Masonry Strength and Openings on Infilled R/C Frames under Cycling Loading. // Journal of Earthquake Engineering. 12, (2008), pp. 197-221.
[5] Eurocode 8: Design of structures for earthquake resistance – Part 1: General rules, seismic actions and rules for buildings. EN 1998-1, CEN, Brussels; 2005.
[6] Eurocode 8: Design of structures for earthquake resistance – Part 3: Assessment and retrofitting of buildings. EN 1998-3, CEN, Brussels; 2005.
[7] Federal Emergency management Agency (FEMA), Evaluation of Earthquake Damaged Concrete and Masonry Wall Buildings, Basic Procedures Manual, ATC-43, FEMA 306, ATC, California, 1999.
[8] Paulay, T.; Priestley, M. J. N. Seismic Design of Reinforced Concrete and Masonry Buildings. J. Wiley and Sons, NY, 1992.
[9] Zovkić, J.; Sigmund, V.; Guljaš, I. Cyclic testing of a single bay reinforced concrete frames with various types of masonry infill. // Earthquake Engineering & Structural Dynamics. 42, 8(2013), pp. 1131-1149.
[10] Zovkić, J. Seismic Behaviour of Reinforced-concrete Frames with Masonry Infill, Josip Juraj Strossmayer University of Osijek; Doctoral Dissertation, 2013.
[11] Crisafulli, F. J.; Carr, A. J. Proposed macro-model for the analysis of infilled frame structures. // Bulletin of the New Zealand Society for Earthquake Engineering. 40, 2(2007), pp. 69-77.
[12] Das, D.; Murty, C. V. R. Brick masonry infills in seismic design of RC frame buildings: Part 2 – Behavior. // The Indian Concrete Journal. August 2004.
[13] Eurocode 2: Design of concrete structures. EN 1992, CEN, Brussels; 2004.
[14] Eurocode 6: Design of Design of masonry structures. EN 1996, CEN, Brussels; 2005.
[15] Sorić, Z. Zidane konstrukcije I, 2. izd. vlast. nakl. Zagreb; 2004.
[16] Tomaževič, M. Earthquake-Resistance Design of Masonry Buildings (Series on Innovation in Structures and Construction - Vol. 1). Imperial College Press, London, 1999.
[17] Crisafulli, F. J. Seismic behavior of reinforced concrete structures with masonry infills. Doctoral Dissertation. 1997, University of Canterbury, Christchurch, New Zealand.
[18] Žarnić, R. Inelastic Model of the R/C frame infilled by Masonry Wall. // Engineering Modelling. 7, 1-2(1994), pp. 47-54.

Authors' addresses

Vladimir Sigmund, prof. dr. sc., dipl. ing. građ.
Josip Juraj Strossmayer University of Osijek
Faculty of Civil Engineering Osijek
Crkvena 21
31000 Osijek, Croatia
E-mail: sigmund@gfos.hr

Jurko Zovkić, doc.dr. sc., mag. ing. aedif.
Josip Juraj Strossmayer University of Osijek
Faculty of Civil Engineering Osijek
Drinska 16A
31000 Osijek, Croatia
E-mail: jzovkic@gfos.hr

Ivica Guljaš, prof. dr. sc., dipl. ing. građ.
Josip Juraj Strossmayer University of Osijek
Faculty of Civil Engineering Osijek
Crkvena 21
31000 Osijek, Croatia
E-mail: iguljas@gfos.hr